Signal Processing Algorithms for Electronic Combat Receiver Applications

Donald E. Maurer, Roxaneh Chamlou, and Kimberly O. Genovese

This article discusses algorithms developed to support improved-sensitivity electronic combat receivers. Fast Fourier transform–based channelization is used to achieve the desired improvement. The algorithms supporting this design also improve the receiver's ability to acquire radar targets having complicated waveforms and enable the receiver to operate with higher pulse densities. On-the-fly parameter estimation assists target classification. These objectives can best be realized in a digital receiver. An acousto-optic design was also explored, and the algorithms developed for the digital design should be applicable to both types of receiver.
(Keywords: Microwave receivers, Digital receivers, Electronic warfare, Signal processing, Automatic target recognition.)

INTRODUCTION

Electronic warfare includes warning, detection, target acquisition, and homing. Critical to its success are support activities such as searching for, intercepting, locating, recording, and analyzing radar signals. The electronic combat (EC) receiver makes these activities against enemy air defense sites possible. EC receivers, for example, are essential components of antiradiation missiles. Figure 1 illustrates a typical engagement. The air-launched antiradiation missile targets a specific emitter in the enemy air defense system. The receiver uses pre-selected electronic intelligence to passively acquire the target. Azimuth and elevation estimates derived from detected signal data guide the missile to the target emitter site. The missile receiver can be

programmed to search for other signals (possibly from the same site) if the primary target cannot be acquired. Thus, an EC receiver must be able to detect as many signals as possible and, therefore, it must have a wide bandwidth, high sensitivity, and dynamic range. Air defense radar emissions often consist of complex pulse patterns and may be frequency modulated; moreover, emitters may have several modes of operation, each having a different waveform. Since the electromagnetic environment (Fig. 1) is becoming more complex in waveform structure and increasing numbers and varieties of emitters, future EC receivers must be capable of fine discrimination and be able to operate in a dense environment. They must be able to process a large
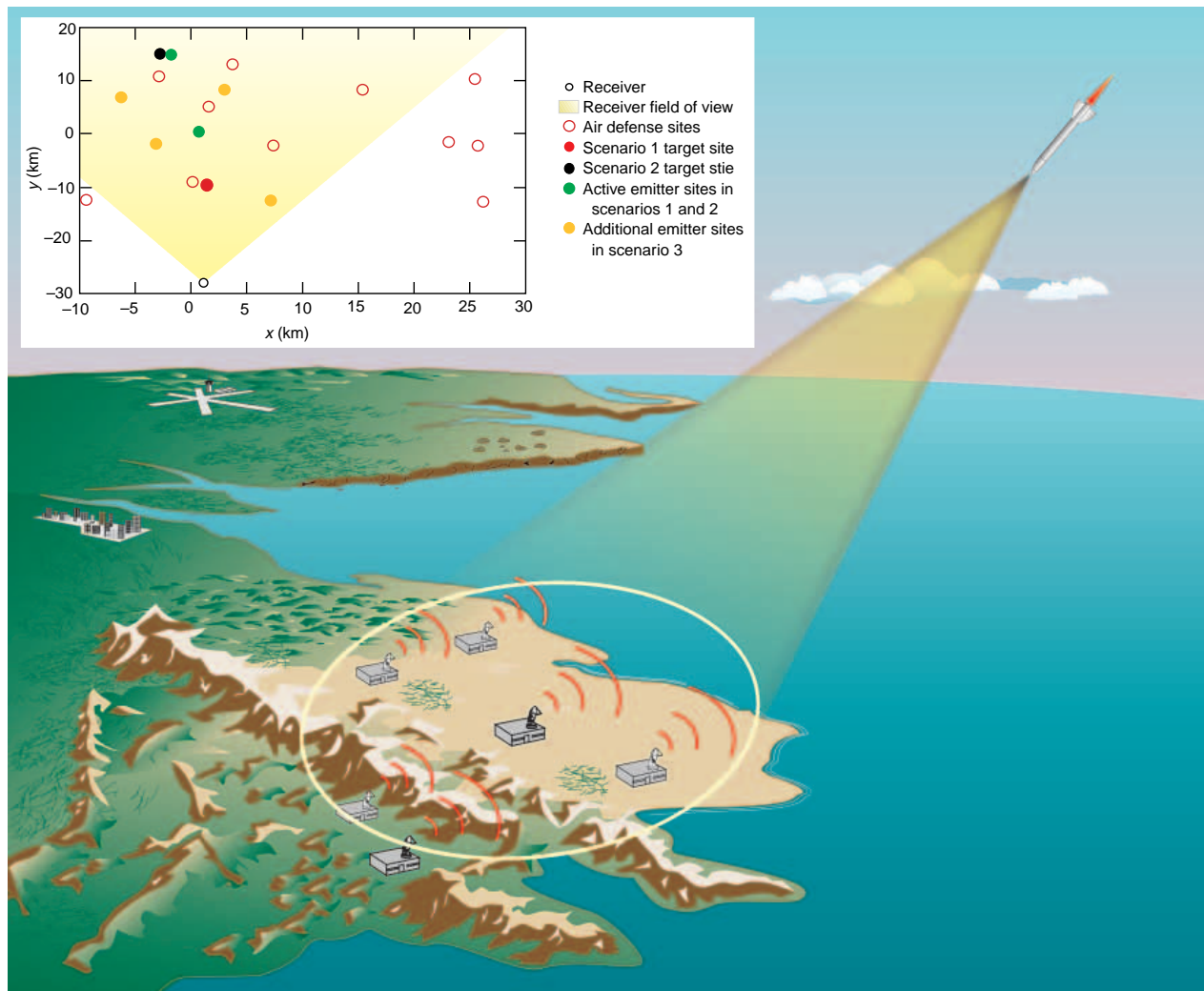
Figure 1. A typical antiradiation missile engagement against an air defense site. The missile receiver must identify waveforms associated with the targeted emitter in a dense electromagnetic environment. The inset shows the cluster of air defense radar sites used in defining scenarios to test the receiver design.

amount of data in a short time. Once a signal has been identified as a target of interest, the receiver should be able to provide information to help locate the signal's source.

APL began a program in the late 1980s to develop signal processing techniques to meet these challenges in future antiradiation missile receivers. Because of the joint nature of this program, the Laboratory's contributions will benefit both the Air Force and the Navy. Objectives of the program were to increase sensitivity by 20 dB over current receivers, improve the ability to acquire radar targets having complicated waveforms, improve on-the-fly parameter estimation and the receiver's ability to use these estimates to assist target classification, and enable the receiver to operate with higher pulse density. A channelized receiver was proposed to achieve these goals.[1] Channelized receivers include compressive, filter bank, acousto-optic, and digital receivers. Technological advances in analog-to-

digital (A/D) converters and digital signal processing provide the possibility of developing a digital receiver. If successful, digital receiver performance may be superior to conventional analog receivers since digital signal processing is more flexible and digitized data can be stored for long periods of time.

The feasibility of implementing channelization with a real-time fast Fourier transform (FFT) was established by several earlier APL studies.[2–4] The major contribution of the authors' design effort, therefore, is the combination of algorithms developed to process the large data stream out of the channelizer. The challenge is to detect target waveform patterns in the digitized output and then maintain contact with the target throughout the missile flight. Many standard pattern classification techniques, however, are too computationally intensive for antiradiation missile receivers; thus, computability is an essential consideration. Although this design was developed and evaluated for

application to antiradiation missile receivers, it can also be adapted to other EC receiver applications, such as intelligence gathering that requires a receiver that can simultaneously process many different waveforms.

RECEIVER SIGNAL PROCESSING DESIGN OVERVIEW

Noise in a receiver is distributed across the entire receiver band, but a radar signal is localized in frequency; therefore, sensitivity can be increased by channelization. If the received signal bandwidth BW is divided into n smaller channels each having bandwidth BW/n, the channel containing the emitter will have less noise but the same signal power, and the signal-to-noise ratio in that channel is increased. After investigating alternative channelization techniques, it was decided that the receiver improvement objectives could best be realized in a digital receiver. (An acousto-optic design was explored, but several problems prevented its implementation.[5] Nevertheless, the target identification and classification algorithms developed for the digital design should be applicable to both types of receiver.) Whereas channelized receivers are more complex than superheterodyne, instantaneous frequency measurement, or crystal video receivers, the advantage of digital

channelizers is their flexibility. Filter shapes can be changed and the analysis bandwidth varied; moreover, a digitized copy of a radar signal can be stored and used as a template or correlator.

Figure 2 consists of two diagrams showing the receiver signal processing. The color coding indicates the level of development of each component. Those that are more complete have been implemented in the Receiver Acquisition Simulation Model (RASM)[6,7]. This model was developed to provide a flexible modular simulation test bed for studying signal processing algorithms. Other signal processing components have been simulated off-line and are still being refined. Figure 2a is an overview of the design, and Fig. 2b highlights the functions required for detection, identification, and classification.

The first block in Fig. 2a shows the antenna, a four-arm spiral providing monopulse direction finding (DF). Spiral antennas are circularly polarized and exhibit nearly constant beamwidth independent of frequency.[8] Thus, low- and high-band frequencies can be received by the same antenna. The four-arm spiral can be excited in two different modes: The sum mode Σ forms a beam pattern with maximum response on the boresight axis, and the difference mode Δ has a beam pattern with a deep null along the boresight. The sum and
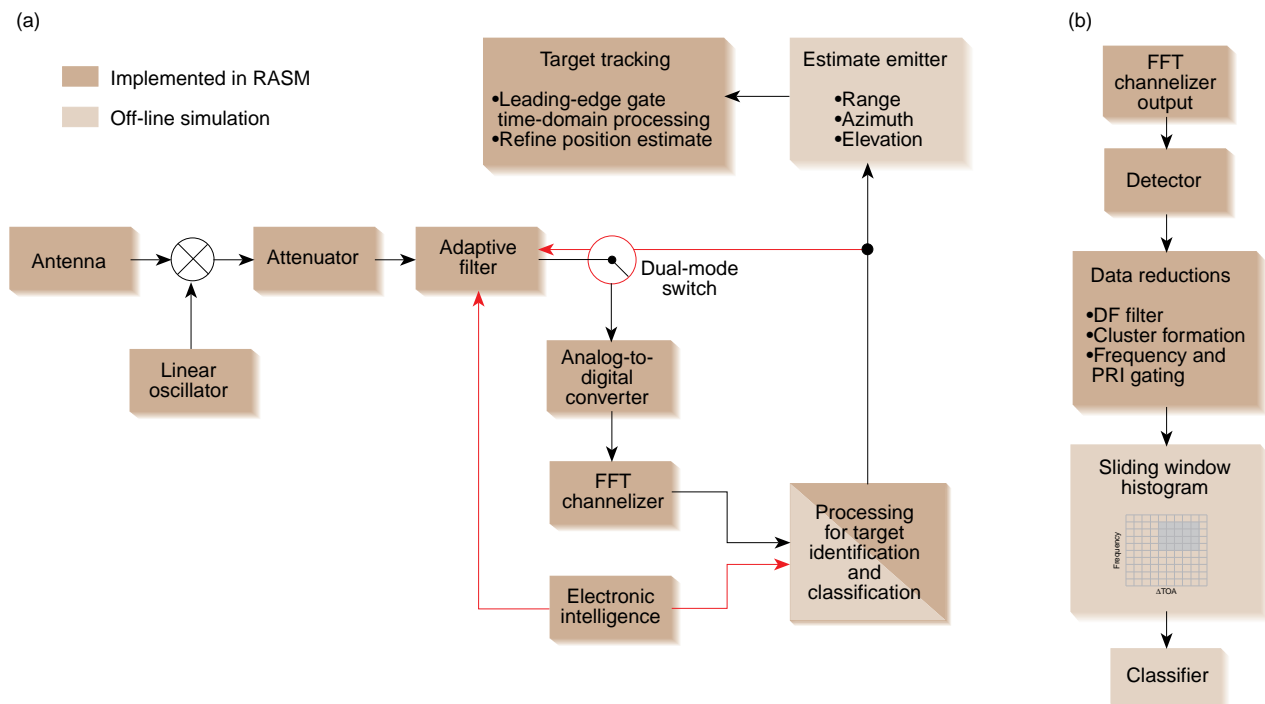

Figure 2. Improved EC receiver functional diagram showing algorithm development stages. Refined algorithms have been implemented in RASM. Less-developed algorithms have been simulated off-line. (a) Signal processing flow diagram. The dual-mode switch optimizes signal processing by switching between channelization when greater sensitivity is required and less intensive signal processing in the time domain otherwise. (b) Detail of the target identification and classification functions.

difference patterns are related such that the azimuth and elevation to a radar source can be estimated by the equations,

$$\text{azimuth angle} = 20\log_{10}\left|\frac{\Sigma + j\Delta}{\Sigma - j\Delta}\right|,$$

and　　　　　　　　　　　　　　　　　　　　　(1)

$$\text{elevation angle} = 20\log_{10}\left|\frac{\Sigma + \Delta}{\Sigma - \Delta}\right|,$$

where j denotes $\sqrt{-1}$.

Figure 2a represents the signal processing functions for both Σ and Δ modes. After converting the signal to an intermediate frequency and attenuating to avoid saturation, an adaptive filter is used to limit the accepted waveforms to a predetermined frequency band, depending on the targets of interest. Electronic intelligence is used in current antiradiation missile receivers to provide these range limits for frequency. EC receivers use this rough frequency information to center the bandwidth. The improved design, however, provides much finer frequency estimates at a later processing stage that can be fed back to the adaptive filter to further reduce the receiver bandwidth, thus attaining additional processing gain for improved tracking and providing a discriminant for target identification. The pulse repetition interval (PRI) is another primary waveform discriminant, but it is not used until the target identification and classification steps in Fig. 2b.

Although the improved design provides more information about radar frequency and waveform structure, the A/D sampling rate limits time resolution to 1 μs (approximate) at the channelizer output. Thus, a pulse with width less than 1 μs cannot be measured accurately. The pulse width (PW), however, is not used as a discriminant, and so this is not a severe limitation for target classification. On the other hand, it is particularly critical regarding multipath-induced DF errors. Monopulse azimuth and elevation estimates are used to guide a missile or track a target. If, however, the pulse is corrupted by overlapping pulses (e.g., from multipath or another emitter), the DF estimates can have a significant error. Because reflections arrive at the receiver after the direct signal, one way to avoid multipath errors is to calculate azimuth and elevation angles using Σ and Δ samples from the leading edge of the pulse before it can be corrupted. This method, however, requires finer time resolution than current FFT technology allows, so we concluded in Ref. 9, after investigating several approaches for resolving the problem including superresolution and differential Doppler

techniques, that a dual-mode receiver offered the best solution.

The dual-mode switch shown in Fig. 2a is used to optimize the signal processing system. The processing gain from channelization and improved acquisition algorithms increase the probability of acquiring the target faster and at greater distance where multipath-induced DF errors are insignificant. If the receiver is close to its target, however, and sensitivity is not an issue, the mode can be switched to less intensive time-domain processing.

Once the target emitter's waveform has been identified and the target has been acquired, a passive location system using the antiradiation missile receiver's position (provided by an onboard global positioning system) could calculate refined target position estimates for guidance or tracking. Preliminary studies of the associative memory technique of Kagiwada et al.[10] showed that their technique can accurately estimate an emitter's position and is feasible to implement. This approach was developed and tested for estimating distance and altitude assuming zero-mean Gaussian DF measurement noise. Although we were able to extend the method to three dimensions, the effect of bias in the DF measurements is still being analyzed.

RECEIVER SIGNAL PROCESSING ALGORITHMS

Channelized receivers have traditionally been implemented with filter bank designs, and efficient hardware realizations of digital filters are available. Alternatively, the set of outputs from the channelizer can be regarded as the Fourier transform of the input signal and realized by an FFT digital processor. These approaches were examined, and after theoretical considerations and a comparison of their computational intensity, it was determined that the specifications for the EC receiver could be achieved effectively with the FFT-based channelizer.[2]

Our design consists of a digital FFT-based channelizer attaining a 20-dB gain in sensitivity and processing a 500-MHz bandwidth with 40-dB instantaneous dynamic range. Since each channel is approximately 1-MHz wide, this technique also improves frequency resolution significantly. This capability is achieved by a 512-point complex FFT that samples the receiver input signal every 2 ns. Sensitivity and bandwidth are limited by the A/D conversion rate. However, fast A/D conversion is critical to many signal processing applications, and efforts to improve performance is continuing in the semiconductor industry.

Figure 3 illustrates the sensitivity of our channelizer design. Figure 3a shows a time-domain segment of a simulated continuous wave (CW) signal from a low-power emitter. The signal is not visible because it is

buried in noise. Detection requires at least a 10-dB signal-to-noise ratio; therefore, this target would be undetectable using time-domain processing. On the other hand, Fig. 3b shows the output of the channelizer. A definite peak, corresponding to the frequency of the target, is visible in bin 256 and could be detected. The gain in performance from this sensitivity improvement is the capability to detect low-power targets at greater range and to obtain more accurate DF estimates.[11]

To take full advantage of the improved sensitivity, but at the same time minimize data processing by limiting false alarms, we implemented an adaptive threshold detector (Fig. 2b) at the channelizer output. In contrast to a fixed-threshold detector, characterized by a strong dependence of the probability of false alarm P_f on the noise power, a constant false-alarm rate (CFAR) detector maintains a false-alarm rate independent of fluctuating background noise by calculating the detection threshold at a specific resolution cell based on a compa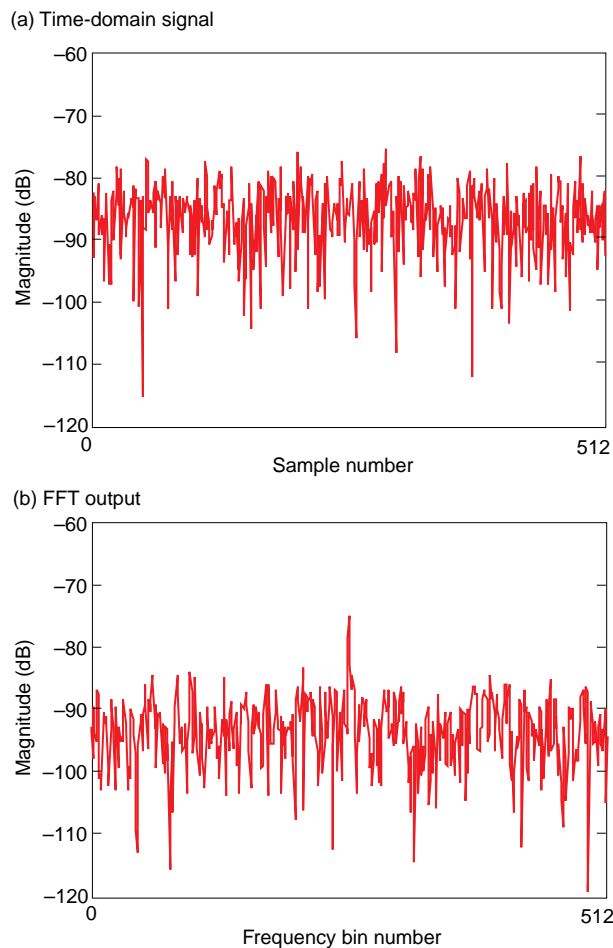rison of its power with the average noise power in a set of adjacent cells. (Variations in noise power are caused by clutter or interference.) This estimate, along with a predetermined scaling factor allowing for uncertainties in the estimate, establishes the adaptive noise threshold.

CFAR detectors differ in how the average noise power is calculated. The ordered statistics (OS-CFAR) method, introduced by Rohling,[12] was chosen over conventional CFAR techniques for its superior handling of the masking or frequency resolution problem. OS-CFAR estimates noise power by taking quantiles rather than the first moments of reference cells. That is, it rank orders the power in the neighboring cells according to magnitude and selects the kth element, where k is a predefined rank-order index. Whereas properties of the OS-CFAR detector are normally derived for a time-domain signal, the only assumption used in their derivation is that the noise is quadrature Gaussian. Since it can be shown that the FFT output will also be quadrature Gaussian, these properties are also valid in the frequency domain. Their validity has also been confirmed through extensive simulations.[13] References 13 and 14 provide more detailed discussions of OS-CFAR.

Figure 4 compares the FFT-channelized output to the OS-CFAR detector threshold with $P_f = 10^{-3}$ for three closely spaced simulated CW signals. The weaker signal can be detected, even when it is in close proximity to stronger signals. This detector was able to distinguish these signals when their center frequencies were as little as 4 MHz apart. Normally, the operating frequencies in an air defense system are separated by guard bands somewhat wider than this. Therefore, the
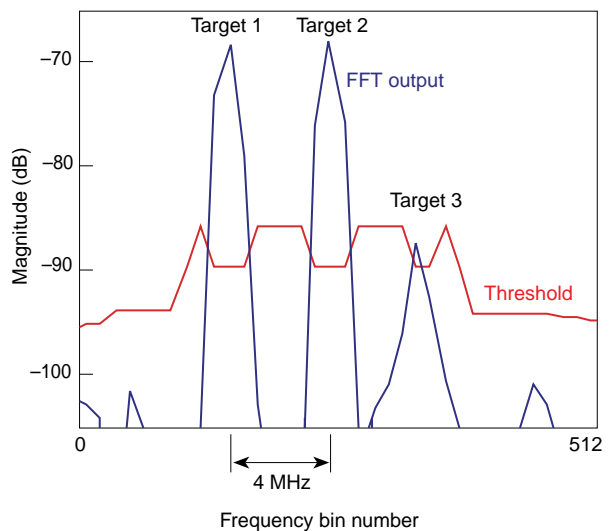

Figure 3. An example showing the sensitivity improvement gained by channelization. (a) A simulated CW signal from a low-power radar buried in noise. (b) After passing the signal through the channelizer, the radar signal appears in frequency bin 256.

Figure 4. Detail of the channelizer output of a simulated signal consisting of three target emitters closely spaced in frequency. The OS-CFAR threshold is superimposed.

designed EC receiver should be able to resolve individual emitters.

The OS-CFAR technique may be too computationally intensive for time-sensitive missile guidance applications. If so, for this application, it may be necessary to trade some sensitivity for increased processing speed. Blais and Rioux[15] discuss an alternative digital peak detector based on differentiating the signal, using a finite-impulse response filter to remove high-frequency noise, and then interpolating the zero crossing to estimate peak location.

The quantity of channelized data to process is further reduced, after detection, by clustering and then using DF as a discriminant.[16] Clustering consists of replacing a set of detections in adjacent frequency bins with the bin containing the output of greatest magnitude. Next, the DF for each cluster representative is calculated. Because the Fourier transform is a linear operator, the equations for azimuth and elevation can be computed on detected FFT output, just as would normally be done on a time-domain pulse. If the DF is inconsistent with previous target position estimates (if available), the cluster is rejected. Generally, the set of cluster representatives could be partitioned into disjoint subsets consisting of those corresponding to specified azimuth and elevation ranges; these subsets could then be processed in parallel to classify *all* detected waveforms passed by the adaptive filter. The waveforms may include a few similar signals from several emitters, or if the intent is to survey the electromagnetic environment, the filter could be opened to admit as many signals as possible.

Once data reduction has been completed, the target must be identified. Since the waveform pattern of each emitter evolves in time–frequency space, some type of pattern matching is an obvious method. Figure 5 shows the time–frequency output after detection and clustering for a 10-ms segment of simulated signal consisting of four different emitter waveforms. Resolution is determined by the FFT parameters: Each cell is 1 μs by 1 MHz. Since the PW of each emitter is less than 1 μs, signal detections cannot be visually distinguished from the false alarms (shown in gray). Therefore, the cells where pulses from the emitters should appear are colored.

Identifying a waveform pattern in time–frequency space poses some difficulty, especially if it is embedded in noise and patterns from other emitters. Two-dimensional histograms are used for further data reduction and to reveal emitter patterns that may not be visible in the time–frequency data. Time-of-arrival (TOA) histogramming is computationally intensive if the differences between every pair of pulses must be calculated to "de-interleave" overlapping signals from different emitters. In the FFT-based design with its narrow channel width, however, the emitter traces will be separated

in frequency. Thus, it should be possible to realize a substantial reduction in computation by using frequency and PRI, or the time-of-arrival difference (ΔTOA) between consecutive pulses (i.e., a *first order* histogram). Other combinations such as frequency vs. PW and PW vs. ΔTOA could be used; however, PW is not a strong discriminant since it can easily be distorted by multipath, and the A/D conversion rate limits the accuracy with which it can be measured.

The shaded portion of the ΔTOA vs. frequency histogram space shown in Fig. 2b represents a limited region defined by the target's estimated frequency and PRI ranges, either from electronic intelligence or refined measurements made by the receiver. Only contributions to histogram cells falling within this restricted region are calculated. As with the adaptive filter, the parameters defining this region can be constrained to eliminate all but a few waveforms or relaxed until the region coincides with the entire histogram space. Furthermore, only cluster representatives falling within the *histogram window*, a time interval large enough to contain a sufficient number of pulses from the target to ensure a valid detection, are used. For a waveform consisting of a simple pulse train, at least six pulses are required to form a histogram in which the probability of a detection error can be made as small as 0.05.[6] However, to account for missing pulses and more complex pulse patterns, a larger histogram window would be required. Histograms are computed sequentially as the window is advanced each time an FFT is calculated: New TOA differences are computed and old ones are dropped. Figure 6 shows the histogram obtained from
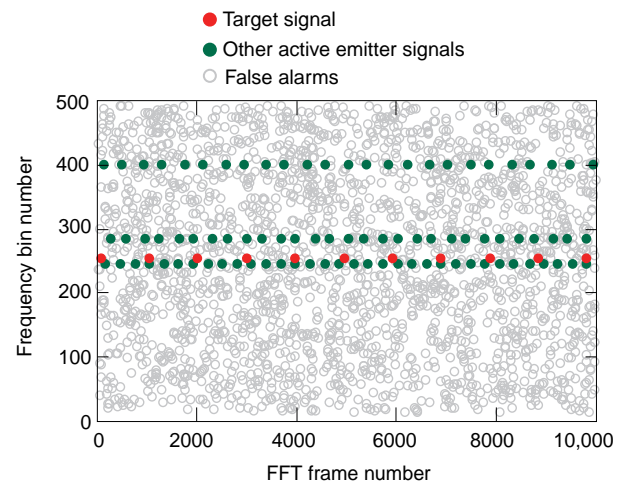

Figure 5. Approximately 10 ms of a simulated signal consisting of four emitter waveforms have been processed, and the detections plotted. A detection is indicated in the *(i,j)*th position whenever the output of the *j*th channel, or frequency bin, exceeds the OS-CFAR threshold. The cells where radar signals should appear have been superimposed in the colors corresponding to the respective emitter sites in Fig. 1. The other (gray) data points are false alarms.
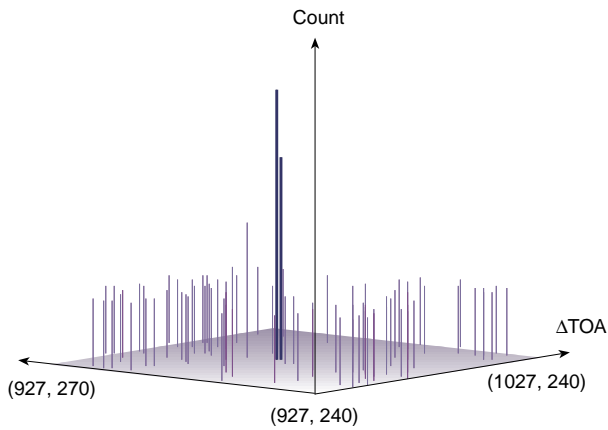
Figure 6. Output of the moving window histogram applied to the signal in Fig. 5 (window length is 40 ms). The magnitude of the spike at an *(x,y)* cell represents the number of pairs of consecutive detections in frequency bin *y* for which ΔTOA = *x*. The (ΔTOA, frequency) coordinates of three corner cells are shown.

processing time–frequency detection data from the simulated signal (see Fig. 5) using a 40-ms histogram window length. The base in the figure corresponds to the shaded region of Fig. 2b and is defined by the (ΔTOA, frequency bin) coordinates of the three corner cells shown in the figure. Each spike represents the content of a histogram cell; the smaller ones are false targets. The spreading associated with the large target peak is caused by slight variations in ΔTOA because the PRI is not an exact multiple of the frame time. For real targets, there may also be spreading because of variations characteristic of the signal generation hardware.

The histogram technique transforms a waveform in time–frequency space into a pattern of densities on the histogram plane. This pattern forms a signature characteristic of the signal type; it may even reflect features of a specific emitter. These histogram patterns must be processed by a classifier to determine whether or not the target is present. The classifier could range from a simple threshold (e.g., the target is present if any histogram cell exceeds the threshold) to an associative memory that can recognize several different histogram distribution patterns. A classifier that keeps track of several modes of the same emitter, or several different emitters, must be more sophisticated than a simple threshold. Template matching[17] and several neural network–based approaches[18,19] were examined. Distributed memory systems appear to be natural for this application. For example, the histogram distribution patterns of eight different waveforms were coded into a three-layer classifier by defining an appropriate set of connection weights and hidden nodes. These weights and nodes were determined heuristically rather than by training the net with back propagation or a similar method. Figure 7 illustrates the procedure for a jittered waveform. Figure 7a displays the parameters defining

jitter, and Fig. 7b illustrates how the histogram characteristics can be represented. Each input node processes the contents of a histogram cell; each of the three 3 × 3 node clusters corresponds to one of the possible ΔTOA values. The clusters model the small variations in ΔTOA that may occur. The green connections activate the hidden node they connect to if

$$x - y + z \geq 0, \qquad (2)$$

where x, y, and z are the histogram densities at the clusters corresponding to $a - 2b$, a, and $a+2b$, respectively. Similarly, the red connections activate the hidden node they connect to if

$$x - y + z \leq 0. \qquad (3)$$

Together, the two inequalities characterize the distribution of ΔTOA values. However, both inequalities also hold if $x = y = z = 0$. The blue connections are intended to eliminate activation in this case. They activate the middle node only after at least four pairs of consecutive pulses with $\Delta TOA = a$ have been processed. Thus, the presence of a jittered waveform is required to fully activate all three hidden nodes. A single output node threshold is determined so that its activation requires the simultaneous activation of each hidden node.

SCENARIOS FOR TESTING THE RECEIVER ALGORITHMS

The signal processing algorithms were tested in the RASM using realistic air defense scenarios designed to stress the algorithm's capability. These scenarios were derived from a database of air defense sites consisting of many radar systems with a variety of waveforms. The radars chosen for our scenarios were from a cluster of sites that provided the greatest variety of systems. The inset to Fig. 1 shows the geographical distribution of this cluster relative to an arbitrary origin. Other radar systems were added to the sites as needed to provide a realistic, complex signal environment for testing. The radars at each site were modeled by parameters that described the waveform (e.g., radar frequency, PRI, PW, and polarization) and propagation characteristics such as power level, pointing angle, beam size, and sidelobe pattern.

The first scenario was devised to test receiver sensitivity against a low-power target. In the Fig. 1 inset, the low-power target site is shown in red. The receiver is on a missile positioned 18.5 km away; its field of view, indicated by the shaded region, contains three emitters—the black and green circles—operating in the same receiver band as the target. These emitters were
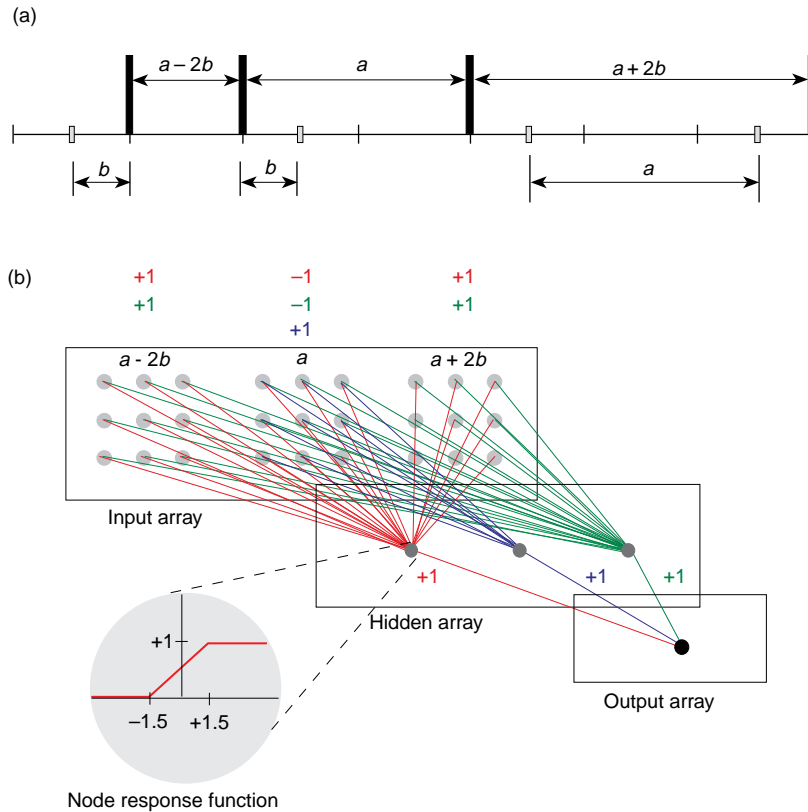
(a)

(b)

Figure 7. Classifier connections and weights for detecting the jittered waveform. (a) Schematic diagram illustrating pulse jitter. Each pulse occurs at an offset of what otherwise would be a fixed PRI of a units. The sign varies randomly from one pulse to the next, so the ΔTOA has three possible values: $a - 2b$, a, or $a + 2b$. Moreover, ΔTOA = a occurs twice as often as either of the other possibilities. (b) Each input node of the classifier corresponds to a histogram cell, and its input is the histogram magnitude. The hidden array consists of three nodes corresponding to the possible ΔTOA values. The response of each hidden node is a ramp function as shown. Connections to the hidden nodes and their weights are color-coded for clarity (weights are listed above the input nodes). The hidden nodes are all connected to a single output node with weight equal to +1.

POST-FFT PROCESSING ALGORITHM TEST RESULTS

This section describes results obtained by testing the signal processing algorithms in the three scenarios of increasing complexity defined in the previous section.

The first scenario was intended to show that with improved sensitivity, the receiver can detect low-power targets at ranges where other antiradiation missile receivers would be ineffective. In this scenario, a radar having a simple pulse waveform and very low power was chosen as the target. With the sensitivity gain realized by the improved receiver design, this target was detected at a range almost 5 times as great as that achievable by current antiradiation receivers. The probability of detection P_d, a simple measure of performance, is the ratio of pulses detected by the receiver to the total number of pulses transmitted. In the first 10 ms of data processed by the new design (Fig. 5), the low-power target had a probability of detection $P_d = 0.90$; in subsequent segments, P_d was lower as the missile passed through antenna nulls and, consequently, several pulses were not detected. As shown in Fig. 6, however, there were enough detections to get a significant peak in the histogram, indicating the target's presence. (When the histogram window length was narrowed to 10 ms, the target was detected initially, but subsequent contact was lost as the frames containing more missing pulses passed through the histogram window and were processed.)

The second scenario was intended to test the receiver's ability to track a target through an operational mode change. If the frequency changes, the target may no longer be in the receiver band. In this case, the band must be tuned to an appropriate intermediate frequency before the emitter can be acquired again. Reference 20 is an exploratory study of a parallel processing technique that promises a significant increase in the bandwidth that can be processed by an FFT without losing sensitivity or increasing the sampling rate. This parallel processing technique has not been tested in RASM.

Even if the frequency of the new operating mode is within the receiver band, the PW and PRI structure may change. This change was examined using the

included to further stress the algorithms. Current antiradiation receivers can detect the low-power target at a range of at most 3.7 km. The ability to maintain contact with the target was tested by a second scenario involving an operational mode change. For the second scenario, the same emitter signals were used as in the first scenario, except that a strong signal with a two-level pulse stagger (shown in black in the inset) was chosen to be the target. In general, an m-level stagger consists of a repeated group of $m+1$ pulses in which the m intrapulse distances, or stagger intervals, are different lengths. The target's second mode had a different pair of stagger intervals and began after 20 ms. A third scenario including multiple targets operating in multiple modes was also defined. This scenario consisted of active emitters located at the eight colored sites in the Fig. 1 inset with frequencies distributed throughout the receiver band. These signals included a jittered pulse, linear frequency-modulated (LFM) pulses, two-level and four-level staggered pulses, and a triple pulse group repeated every 80 ms.

stronger two-level pulse stagger signal defined in the second scenario. The moving histogram window length was chosen wide enough (10 ms) to include a sufficient number of pulses to calculate the double-peak histogram signature of two-level stagger. When the first 10 ms of signal data was processed, the two peaks characteristic of the first mode appeared (Fig. 8a). As the signal passed through the histogram window, the mode change was observed (Fig. 8b). First, indications of both modes appeared, but the peaks were small because no more pulses were being transmitted in the first mode and the second mode was just beginning; finally, all traces of the first mode disappeared and the second mode could clearly be detected (Fig. 8c). When the classifier was a simple threshold, the target was lost during part of the mode change. The distributed memory classification algorithm, however, was able to keep track of the target throughout the mode change.

The objective of the third scenario was to see how well individual emitters could be distinguished in a relatively dense signal environment. The distributed memory classifier was used. Histogram patterns for each of the eight-emitter waveforms were coded similar to the jittered waveform example, using appropriate electronic intelligence cueing; there were eight output nodes, each corresponding to one of the emitters. Experiments with this scenario were encouraging. Each signal was correctly classified. However, more work needs to be done to determine an appropriate architecture in which to implement this classifier. Reference 21 is a promising approach.

In all tests so far, target detection has been successful, although when the target signal is LFM, or chirped, the resulting frequency spread can mask signal indications that are nearby in time-frequency space; moreover, since the energy is spread over a wide frequency band, its spectral peak is lowered and consequently its detectability reduced. An option for processing LFM signals was proposed in Ref. 22. This option uses a variable offset correlator to compress the energy in a chirp into a single frequency bin. Although theoretical studies have been encouraging, the technique has not yet been implemented in RASM.

CONCLUSIONS

An improved digital channelized receiver design has been defined, and algorithms for the functional components have been developed. The performance
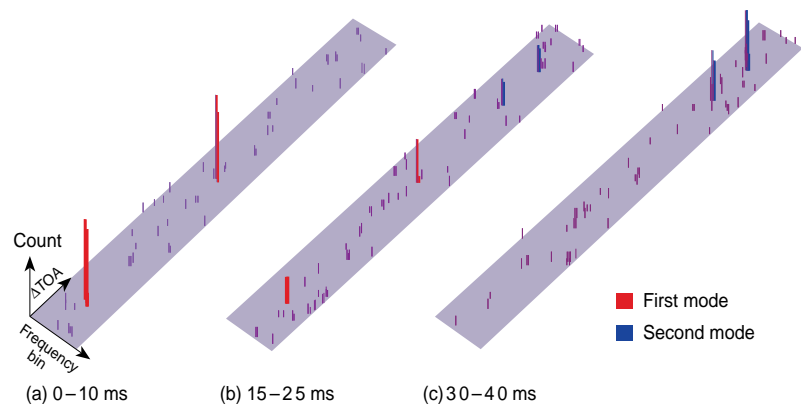

Figure 8. Three views of the moving histogram window (window length is 10 ms) for scenario two. Each histogram is derived from 10 ms of signal data and limited by operationally realistic estimates of frequency and stagger parameter ranges. (a) The first mode. (b) Transition from the first to second mode. (c) The second mode.

(a) 0–10 ms   (b) 15–25 ms   (c) 30–40 ms

advantages include increased sensitivity, ability to process complex waveform types, and operation in a dense emitter environment. The frequency and pulse structure of an emitter can be extracted from the histogram signature and used to tune the adaptive filter, or stored as a template for future target identification. This design was successfully tested in simulations against a single low-power target operating in a single mode and a single target with a mode change, and in a scenario consisting of multiple in-band targets. These simulation studies are the first step in assessing the feasibility of the design. To develop a hardware prototype, however, more work needs to be done, including further development of the algorithms explored in several of the references.[20–22] The storage capacity of the distributed memory classifier needs to be determined and compared with operational requirements before making a final judgment on its suitability for EC receiver applications. Moreover, an appropriate computational architecture remains to be identified to realize the design in real time.

REFERENCES

[1] Lehnus, D. S., and Hartranft, J. F., *Preliminary Feasibility Assessment of a Broadband FFT-Based Channelized Receiver*, F1D-3-90U-012, JHU/APL, Laurel, MD (May 1990).
[2] Shiflett, G. D., *Dynamic Testing of High-Speed Analog-to-Digital Converters*, F1D-93-3-048R, JHU/APL, Laurel, MD (Nov 1993).
[3] Shiflett, G. D., and Maurer, D. E., *A Comparison of the Discrete Fourier Transform and the Polyphase Filter Methods of Implementing a HARM Digital Filter Bank*, F1D-2-91U-041, JHU/APL, Laurel, MD (Dec 1991).
[4] Ardeshna, A. V., *Analysis of Alternate Architectures for FFT-Based Receiver*, F1D-2-91U-077, JHU/APL, Laurel, MD (Dec 1991).
[5] Scoville, M. A., *Acousto-Optic Channelizer Work Status*, F3A(1)-92-186, JHU/APL, Laurel, MD (Aug 1992).
[6] Maurer, D. E., *HARM Acquisition Simulation Model (HASM)*, FS-91-087 (Rev. 1), JHU/APL, Laurel, MD (Apr 1991).
[7] Ardeshna, A. V., *FFT Integration into the HARM Acquisition Simulation Model (HASM)*, F1D-2-91U-047, JHU/APL, Laurel, MD (Jul 1991).
[8] Corzine, R. J., and Mosko, J. A., *Four-Arm Spiral Antennas*, Artech House, Inc., Norwood, MA, pp. 5–36 (1989).
[9] Maurer, D. E., *Electronic Combat Design Techniques for Resolving Multipath*, F3A-94-155, JHU/APL, Laurel, MD (Jul 1994).

[10] Kagiwada, H. H., Kagiwada, J. K., and Kalaba, R. E., "Associative Memories for Third-Generation Passive Ranging," *Computers Math. Applic.* **21**, 81–85 (1991).

[11] Chamlou, R., *Simulation Results for the FFT Channelized Receiver*, F3A(3)-92-201, JHU/APL, Laurel, MD (Aug 1992).

[12] Rohling, H., "Radar CFAR Thresholding in Clutter and Multiple Target Situations," *IEEE Trans. Aerosp. Electron. Syst.* **AES-19**, 608–621 (1983).

[13] Chamlou, R., *Spectral Applications of the OS-CFAR Technique for Target Detection in a Digital FFT Channelized Receiver*, F3A-93-156-R, JHU/APL, Laurel, MD (Jan 1994)

[14] Levanon, N., *Radar Principles*, John Wiley and Sons, Inc., New York, pp. 256–263 (1988).

[15] Blais, F., and Rioux, M., "Real-Time Numerical Peak Detector," *Signal Processing* **11**(2), 145–155 (1986).

[16] Chamlou, R., *Summary of Detection and Data Reduction Algorithms*, F3A(1)-93-249, JHU/APL, Laurel, MD (Sep 1993).

[17] Maurer, D. E., *New Electronic Combat Receiver Design Techniques for Identifying Emitter Waveforms in Time-Frequency Space*, F3A-93-243-R, JHU/APL, Laurel, MD (Oct 1993).

[18] Lipmann, R. P., "Pattern Classification Using Neural Networks," *IEEE Commun. Mag.* **27**(11), 47–64 (1989).

[19] Anderson, J. A., Gately, M. T., Penz, P. A., and Collins, D. R. "Radar Signal Categorization Using a Neural Network," *Proc. IEEE* **78**(10), 1646–1657 (1990).

[20] Maurer, D. E., and Sadowsky, J., "An Algorithm for Estimating the Frequency of a Sub-sampled Signal Using the Chinese Remainder Theorem," in *Proc. 27th Conf. on Information Sciences and Systems*, The Johns Hopkins University, Baltimore, MD, pp. 645–649 (1993).

[21] Saarinen, J., et al., "Highly Parallel Hardware Implementation of Sparse Distributed Memory," in *Artificial Neural Networks*, T. Kohonen, K. Makisara, O. Simulu, and J. Kangas (eds.), Elsevier Science, New York, pp. 673–678 (1989).

[22] Maurer, D. E., *Generalized Correlation Processing with Applications to Electronic Combat Receiver Design*, F3A-94-244, JHU/APL, Laurel, MD (Oct 1994).

THE AUTHORS

DONALD E. MAURER is a member of the Senior Professional Staff in APL's Power Projection Systems Department. He holds a B.A. from the University of Colorado and a Ph.D. from the California Institute of Technology. Before joining APL in 1982, he held positions at the Institute for Defense Analyses and the Center for Naval Analyses. At APL, Dr. Maurer has been involved in modeling, simulation, and algorithm development in support of various programs. Most recently, he has developed acquisition and target detection algorithms for the High-Speed Antiradiation Missile Receiver Sensitivity Improvement Program. Dr. Maurer is a member of the American Mathematical Society, the New York Academy of Sciences, and the Society of Sigma Xi. His e-mail address is Donald.Maurer@jhuapl.edu.

ROXANEH CHAMLOU is a member of the Senior Professional Staff in APL's Air Defense Systems Department. She received her B.S. and M.S. degrees in electrical engineering from the University of Maryland in 1980 and 1982. Since joining APL in 1986, she has worked on modeling, simulation, and algorithm development of a target tracker and predictor for the AN-SPY-1B radar; modeling, simulation, and algorithm development of a prototype detector for the Defense Suppression Program; and early warning timeline analysis and modeling of search area for cued threat acquisition for the Tactical Ballistic Missile Defense (TBMD) Program. Her e-mail address is Roxaneh.Chamlou@jhuapl.edu.

KIMBERLY O. GENOVESE is a member of the Associate Professional Staff in APL's Power Projection Systems Department. She received B.S. and M.S. degrees in applied mathematics from Virginia Polytechnic Institute and State University in 1989 and 1991, respectively. Since joining APL in 1991, Ms. Genovese has worked on a variety of projects including the USAF Defense Suppression Program, the Common Network Planning Software Program, the Battle Group Strike Coordination Program, an Independent Research and Development project in Distributed Correlation and Tracking, the Resource Allocation and Investment Decision Support Program, the High-Altitude UAV Surveillance Capability project, the Tomahawk Baseline Improvement Program, and the Tactical Ballistic Missile Program. Her activities include analysis, software and algorithm development. She is currently working on algorithms for the Data Distribution System of the Cooperative Engagement Capability Program. Her e-mail address is Kimberly.Genovese@jhuapl.edu.